TRACK ASSOCIATION PERFORMANCE OF THE BEST HYPOTHESES SEARCH METHOD

J. A. Siminski[(1)], H. Fiedler[(1)], and T. Schildknecht[(2)]

[(1)]*Space Situational Awareness, German Space Operations Center, Deutsches Zentrum für Luft- und Raumfahrt, 82234 Weßling, Germany, Email: {jan.siminski, hauke.fiedler}@dlr.de*
[(2)]*Astronomical Institute, University of Bern, 3012 Bern, Switzerland, Email: thomas.schildknecht@aiub.unibe.ch*

ABSTRACT

Uncontrolled space objects in the geostationary orbit domain are hazardous threats for active satellites. Catalogs need to be build up, in order to protect this precious domain. The Swiss ZimSMART telescope, located in Zimmerwald, regularly scans the geostationary ring in order to provide a homogenous coverage. This surveying technique typically yields short measurement arcs, called tracklets. Each tracklet provides information about the line-of-sight and the rates of change but typically not about the full state of the observed object. Computationally intensive multi-hypothesis filter methods have been developed to associate tracklets with each other. An effective implementation to this approach is presented that uses an optimization algorithm to reduce the number of initial hypotheses. The method is tested with a set of real measurements of the aforementioned telescope.

1. INTRODUCTION

Debris populating the geostationary orbit poses a threat to active satellites. The unique characteristics of this orbit makes it essential for communication, broadcasting, navigation and weather surveillance. It is therefore of great importance to maintain the usability by building up a catalog with ephemeris data.

The Astronomical Institute of the University of Bern (AIUB) developed the robotic telescope ZimSMART that monitors the geostationary orbit domain from ground. Single objects are not tracked individually but instead the complete region is surveyed in order to built up a catalogue [4]. This survey yields short sequences of angle measurements, called tracklets, that cover a small fraction of the overall orbit. Due to the short coverage, these tracklets lack of complete state information.

They are therefore associated to already cataloged objects or, if no known matching object is found, tested pairwise with other observations [2]. This work focuses on the latter problem, where it is tested whether two tracklets belong to a common object or not. If they belong to each other, an initial orbit state must be determined for a candidate catalog object.

Milani et al. [8] and Tommei et al. [11] suggested to bound all possible orbit solutions for a tracklet to an admissible region by physical constraints, e.g. requiring that a candidate object can only be on a stable orbit around the Earth. The admissible region concept was utilized by several researchers in their approaches to link observation arcs. Fujimoto et al. [3] find the common orbit solution of two tracklets by computing the overlap of both possible solution spaces. They, therefore, fill each admissible region with state hypotheses and propagate them to a common epoch for comparison.

Another approach, proposed by DeMars et al. [1], is to sample only the region of one tracklet with a bank of hypotheses and propagate each one to the epoch of another tracklet. Each hypothesis is then tested with the new observation. If the test fails, i.e. the hypothesis does not match the other observation, it is removed. However, if a hypothesis survives the gating process, a candidate object is created whose orbit can be affirmed and refined with further observations.

Both methods require a complete sampling of the admissible region with hypotheses to guarantee that each possible orbit solution is tested. As each hypothesis, i.e. a state and its associated uncertainty, needs to be propagated, the sampling density effectively defines the computation time. Therefore, an efficient iso-energy-grid has been proposed in [10] to decrease the computational effort of the hypothesis testing. Additionally an optimization algorithm is used to search for the best fitting hypothesis instead of testing all possible ones.

This paper will shortly summarize the research on the iso-energy-grid and hypothesis search and then assess its performance. The approach is tested using measurements from the ZimSMART robotic telescope. The provided set contains measurements of two following nights, which will be used to evaluate the association performance.

Proc. '6th European Conference on Space Debris'
Darmstadt, Germany, 22–25 April 2013 (ESA SP-723, August 2013)

2. BACKGROUND THEORY

This section summarizes the methodology that is used to perform a track association. Firstly, optical measurements and their derived quantities are discussed. Then, the new approach of using an iso-energy grid and a search algorithm will be outlined.

2.1. Observations

When operating the telescope in a survey-only mode, it captures short sequences of astrometric observations of an object, i.e. right ascension α and declination δ values in a topocentric reference frame

$$\alpha_i, \delta_i, t_i \quad \text{for} \quad i = 1, \ldots, n \quad \text{, where } n \geq 3.$$

In view of the short duration, the information in this tracklet is not sufficient to determine the full set of orbital elements of the object. Therefore the information is merged into a so-called attributable vector, which contains the line-of-sight direction and its derivative

$$\boldsymbol{a} = (\alpha, \dot{\alpha}, \delta, \dot{\delta}). \tag{1}$$

A quadratic or linear polynomial, which models the change in angles over time, is fitted to the observations (cf. [7]). Similarly to the tracklet, the 4-dimensional attributable vector does not itself provide enough information to determine a full set of six orbital elements. However, when combining the attributable with a range and range-rate hypothesis $(\rho, \dot{\rho})$, the state vector

$$\boldsymbol{y} = y(\rho, \dot{\rho}, \alpha, \dot{\alpha}, \delta, \dot{\delta}) \tag{2}$$

or, equivalently, the orbital elements become uniquely defined. The space of orbit solutions for one measurement is then bounded by restricting the possible range and range-rate combinations with the admissible region concept.

2.2. Admissible Region

The admissible region defines the space of possible range and range-rate combination and can be limited using physical constraints [8, 11]. These constraints can be set up by requiring that candidate objects are on stable orbits around the Earth and should not deorbit withing the next revolutions. Therefore, the orbital energy of the hypothesis state must be non negative and the perigee height must be above a certain limit. After transforming the state from the topocentric coordinate system into the inertial one, the energy can be obtained. The specific energy of an object at the geocentric position $\boldsymbol{r}$ with the velocity $\boldsymbol{v}$ is defined as:

$$\mathcal{E} = \frac{\|\boldsymbol{v}\|^2}{2} + \frac{\mu}{\|\boldsymbol{r}\|}. \tag{3}$$

An illustrative example admissible region boundary is shown in Figure 1, where the energy was required to be non-negative and a minimum perigee height was used. It also shows lines of equal energy or semi-major axis respectively.

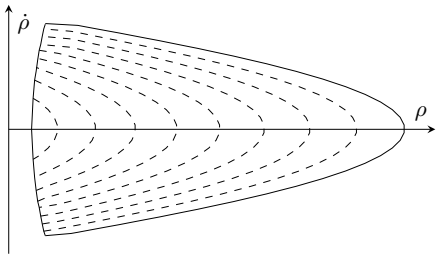

Figure 1. Illustration of the Admissible Region *boundary. The energy of the orbit solutions stays constant on the dashed lines.*

The extent of the region can be furthermore restricted by allowing only solutions in a specified orbital region, e.g. when only the near-geostationary region is of interest. This can be achieved by restricting the orbital energy by certain bounds. Constraining the semi-major axis from both sides will lead to a banana shaped region as illustrated by a pair of dashed lines in the shown figure.

2.3. Hypothesis testing

Without any prior knowledge, all possible state hypotheses $(\rho_0, \dot{\rho}_0)$ of one attributable $\boldsymbol{a}_0$ at the epoch t_0 are equally likely. In order to identify whether a second observation $\boldsymbol{a}_1$ at t_1 belongs to the same object as the initial one, the possible range and range-rate combinations must be tested. Therefore, the probability for a hypothesis to be a common solution of both attributables must be computed. As a measure for this probability the so-called Mahalanobis distance is evaluated [1]. It is effectively the distance between a hypothetical measurement $\hat{\boldsymbol{a}}_1$ at the epoch t_1 and the actual measurement $\boldsymbol{a}_1$ weighted with the uncertainties $\hat{\boldsymbol{C}}_1$ and $\boldsymbol{C}_1$. The quantities $\hat{\boldsymbol{a}}_1$ and $\hat{\boldsymbol{C}}_1$ are the propagated initial attributable $\boldsymbol{a}_0$ and covariance matrix $\boldsymbol{C}_0$ using a measurement and propagation model as well as the orbit hypothesis (cf. [1]). The uncertainties of the attributables are assumed to be normally distributed and are thus described by the respective covariance matrices. The corresponding loss function is given by

$$L\left(\rho_0, \dot{\rho}_0\right) = \Delta \boldsymbol{a}_1{}^{\top} (\hat{\boldsymbol{C}}_1(\rho_0, \dot{\rho}_0) + \boldsymbol{C}_1)^{-1} \Delta \boldsymbol{a}_1, \tag{4}$$

where

$$\Delta \boldsymbol{a}_1 = \boldsymbol{a}_1 - \hat{\boldsymbol{a}}_1(\rho_0, \dot{\rho}_0). \tag{5}$$

In order to obtain the best fitting range and range-rate hypothesis, the above shown loss function must be minimized.

The distance itself is a random variable and distributed according to the χ^2 distribution. It can therefore be gated using a predefined significance level (cf. [1]).

Figure 2 shows the loss function for an example case, where the same object is re-observed after two nights. If the attributables do not match, i.e. if two different objects were observed, the loss function looks quite similar. However, the global minimum of the loss function will be larger than in the case of one observed object.

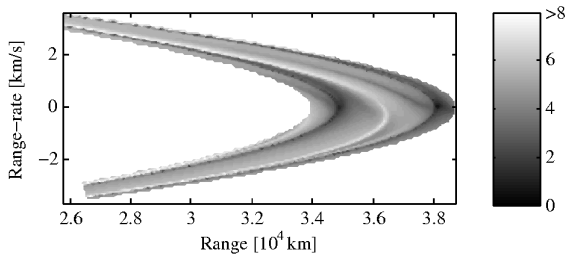

Figure 2. $\log_{10}$ *of the loss function for the admissible region bounded by the semi-major axis from both sides (30000km - 45000km). Two tracklets of the same geostationary communication satellite from the AIUB database were chosen. The time interval between the initial tracklet and the second one is 1.9 days*

The topography of the loss function is analyzed to determine a strategy for minimization. Several local minima can be observed that might contain the common orbit solution of both attributable vectors. The number of the feasible areas increases with the number of possible orbit revolutions between the two measurement epochs. The latter number can be derived from the time interval between the epochs and the semi-major axis limits. That also implies, that the region can be potentially sectioned using the orbital period or semi-major axis in order to obtain subregions with, ideally, only one feasible solution. Due to the uncertainties of the measurements, many of these feasible areas can actually contain probable ambiguous orbit solutions. The larger the time interval between the epochs is, the more of these ambiguous solutions can be found. It can be concluded, that the admissible region must be sampled denser for longer time intervals than in case of a re-observation within the same night. The computational burden increases with the number of loss function calls, as each call includes propagating the hypothesis state and its uncertainty. To avoid a complete admissible region sampling and therefore large computational efforts, a search method is presented in section 2.5 that reduces the number of function calls.

2.4. Iso-Energy-Grid

The admissible region is traditionally discretized on a rectangular grid or using a Delaunay triangulation [11]. As these grids do not consider the topography of the loss function, they require dense sampling to account for every possible solution. To cope with this problem, an alternative grid is proposed. Figure 3 illustrates the coordinate transformation from one grid to the other. Instead of

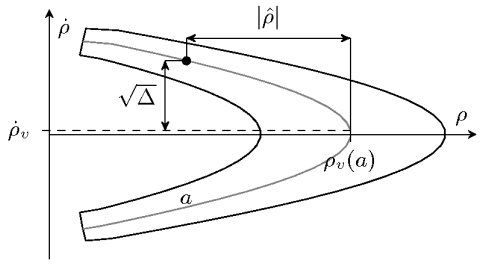

Figure 3. Illustration of the iso-energy coordinate transformation

using the range and range-rate, the semi-major axis and relative rate $\hat{\rho}$ are used. The latter will be explained in the following. The energy Equation (3) is quadratic in the range-rate variable. If semi-major axis and range are given, the equation can be solved for its roots in order to determine range-rate solutions. If the discriminant Δ of the quadratic function is positive, two solutions can be found:

$$\dot{\rho}_{1,2} = \dot{\rho}_v \pm \sqrt{\Delta}, \tag{6}$$

where $\dot{\rho}_v$ is the vertex range rate and constant for all energy levels. The range value ρ_v is the intercept of the iso-energy line with the vertex axis, i.e. the uppermost point of an iso-energy line. The absolute value of the relative range is then the difference between the range and ρ_v. The sign of the relative range is used to define which of the two solutions in Equation 6 is wanted.

Using the mentioned values, a coordinate transformation from the range and range-rate space $(\rho, \dot{\rho})$ to a semi-major axis and relative range space $(a, \hat{\rho})$ can be mathematically expressed by:

$$\hat{L}\left(a, \hat{\rho}\right) = L\left(\rho(a, \hat{\rho}), \dot{\rho}(a, \hat{\rho})\right), \tag{7}$$

where

$$\rho(a, \hat{\rho}) = \rho_v(a) - |\hat{\rho}| \tag{8}$$

and

$$\dot{\rho}(a, \hat{\rho}) = \begin{cases} \dot{\rho}_v - \sqrt{\Delta}(a, \rho), & \text{if } \hat{\rho} < 0 \\ \dot{\rho}_v, & \text{if } \hat{\rho} = 0 \\ \dot{\rho}_v + \sqrt{\Delta}(a, \rho), & \text{if } \hat{\rho} > 0 \end{cases} \tag{9}$$

Figure 4 shows the loss function for the same example case as in the figure with the traditional admissible region coordinates.

The iso-lines can alternatively be sampled with an equidistant grid, i.e. the secant length

$$\sqrt{\Delta\rho^2 + \Delta\dot{\rho}^2}$$

between neighboring hypothesis points stays constant. A method to determine this equidistant grid is described in

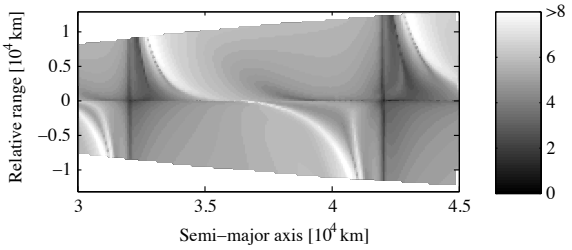

Figure 4. Loss function using the same tracklets and bounds as in Figure 2 but on the iso-energy grid.

[10]. The advantage of using a coordinate transformation instead of discretized grid is, that also line minimization methods can be used, as e.g. given in [9].

2.5. Minimum search

The loss function can be seen as a topography, where the global minimum represents the best hypothesis. Numerical methods can be exploited in order to find it, e.g. the downhill simplex search or evolutionary multi-modal optimization methods (see [9]). Here, a pattern search is implemented due to its simplicity and robustness. [6] describes the formal concept of a pattern search. The loss function $L(\rho, \dot{\rho})$ in Equation 4 shall be minimized. Given an initial value inside the admissible region, its surrounding area is tested with exploration moves in a specific distance. The move, that returns the best improvement, i.e. the smallest loss function value, is used as the new initial search point. If none of the surrounding points is better than the middle one, the search distance, or step size respectively, is reduced. The search is an iterative process, which stops when a predefined convergence criterion is reached, e.g. the loss function or step size becomes smaller than the accuracy requirement. The region should be explored in the most promising directions, i.e. directions that can most probably lead to improvements. The topography of the loss function contains valleys and hills, that are approximately distributed along the different energy levels. Therefore, testing a hypothesis with a different energy should lead to a change, positive or negative, in the loss function. Additionally the algorithm can walk across the iso-energy lines by altering the range value. As described in section 2.3, the loss function can contain multiple feasible orbit solutions. Consequently, the region is beforehand sectioned into smaller subregions, where each subregion optimally contains only one minimum. However, it is not guaranteed that the feasible valleys stay inside a section. That is why each section is individually sampled with an sufficient amount of equally distributed start points. If a search does not reach a feasible area within a certain number of steps, it is dropped. Surviving search results, i.e. the local minimum solutions, are afterward tested with a threshold. If no result passes this gate, it can be concluded that the measurements do not share a common space object. The sectioning process is described in detail in [10].

3. RESULTS

As already written in the introduction, the AIUB provided a set of measurements of the ZimSMART (Zimmerwald SMall Aperture Robotic Telescope) telescope. The telescope is located in Zimmerwald, close to Bern in Switzerland and is used to build up a catalog of objects in the geostationary orbital region.

Figure 5. Set-up of the ZimSMART telescope. Credits to Astronomical Institute University of Bern

The accuracy of the measurements of the telescope is about one arcsecond [5]. The error can be a good assumption for the individual angles but can lead to large errors in the derived rates. It also contains systematic terms that are similar for all observation in one tracklet, e.g. caused by errors in the star catalog or wrong calibration. Consequently, the relative error between the individual measurements can be much smaller, which leads to better error estimates for the angle rates. The time duration of one tracklet is around two minutes, with approximately five individual measurements per tracklet. While computing the attributable vectors, i.e fitting the angular motion model to all 180 tracklets, also the residuals for each linear fit can be determined. The resulting root mean square (RMS) values of the residuals for all tracklets are shown in Figure 6 and 7.

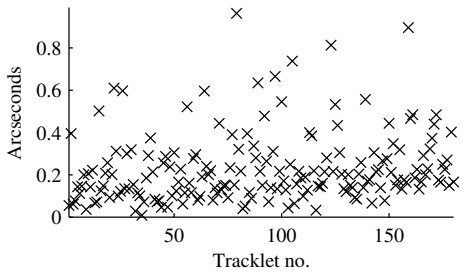

Figure 6. RMS values of the right ascension linear fit residuals within one tracklet for all 180 observed tracklets.

Five independent measurements in one tracklet are not sufficient to provide a good estimate of the actual relative error but can be used conservatively in the association process. It can be observed, that the spread of RMS

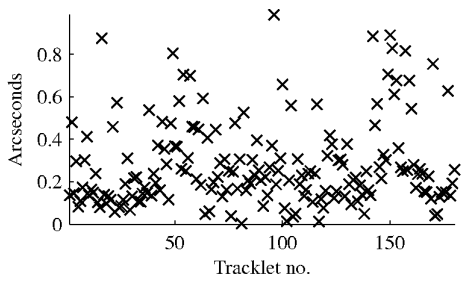

Figure 7. RMS values of the declination linear fit residuals within one tracklet for all 180 observed tracklets.

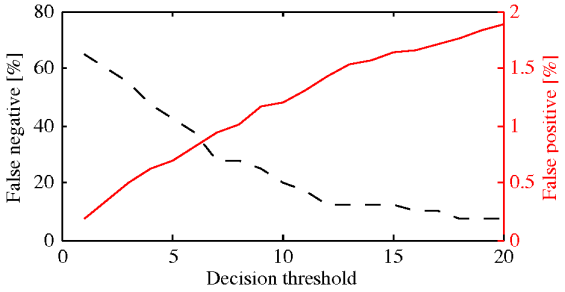

Figure 8. False positive and false negative ration dependent on the maximum allowed distance between the propagated initial measurement and the second one.

values in the figures is smaller than the beforementioned arcsecond. For the determination of angle rates, the relative error is therefore conservatively assumed to be 0.4 arcseconds for both angles.

The method is evaluated using a set of 180 tracklets taken in two consecutive nights. The tracklets were associated to known objects by the AIUB. 40 objects were observed two times and the remaining 100 tracklets belong to indiviual objects. In total approximately 16000 tracklet combinations must be tested, where 40 combination should return a positive match and the rest should be identified as distinct objects by the algorithm.

The evaluation is performed on a Intel Core i7-3720 CPU with 2.60 GHz clock rate. Each hypotheses search takes around 0.7 seconds, which adds up to 3.1 hours for the complete data sample. The run-time varies from one tracklet combination to the other depending on the topography of each loss function. The smaller the time interval between the tracklets, the less initial search points are required to cover the complete region. The bounding semi-major axis values of the admissible region can furthermore be used to reduce the computation time. For the statistics shown here, the semi-major axis was required to be between 38000 and 45000 km.

In [10] it is presented that the here used pattern search requires up to three orders less function evaluations than the traditional complete sampling.

The tracklet association performance is tested by evaluating the number of erroneous decisions for observations of non-common objects and the number of erroneous decisions for observations of common objects. The first can also be described as the false positive associations and the latter are the false negative ones. The statistics of this performance test is shown in Figure 8, where the percentage of false negatives and false positives are shown w.r.t. to a threshold value.

One can observe that most tracklets that actually belong to each other were successfully associated, while keeping the rate of erroneous associations of distinct objects low. One remaining tracklet pair could not be paired correctly. The reason could be an unknown maneuver or a bad measurement. As written in section 2.3, the association gate can consider that the return of the loss function should be distributed according to the χ^2 distribution.

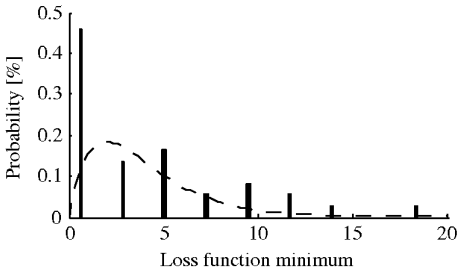

Figure 9. Distribution of distance values for tracklets that belong to common objects.

Figure 9 shows the minimum loss function values, i.e. distances, for all tracklet pairs of common objects and the corresponding $\chi^2(4)$ distribution for 4 degrees of freedom. While the tail of the distribution appears well represented, the distribution peak does not meet the expectations. In so, the presented statistics suffer from the small number of observations belonging from common objects (40). The above mismatch indicates inappropriate assumptions on the employed measurement statistics and a careful reassessment of observation errors is deemed necessary as part of future research.

4. SUMMARY AND CONCLUSION

An extension to the multi-hypothesis testing approach to identify common objects in a database of tracklets was presented. The region of feasible orbit candidates is searched for the best fitting one. The search moves on an efficient iso-energy grid that incorporates the topography of the loss function. In addition to previous research, which mainly focused on the run-time, this work focused on the actual association performance. Therefore, a set of measurements provided by AIUB was processed. The common objects in the given data could be successfully identified, while keeping the rate of erroneously detected objects low. This work furthermore

questioned how tracklet uncertainties should be retrieved. A simple error model, where each tracklet has a constant error term in addition to the individual measurement errors, was shown to be more accurate. Nevertheless, the error modeling must be studied more in detail in future work. The here used database could only evaluate the errors for one known object. Additionally, strategies need to be invented on how to set the gating thresholds. Large thresholds can help to link observations of the same object but also lead to large false positive rates. Unnecessary non-realistic combinations of tracklets lead to a large database of possible catalog candidates, which ultimately leads to a large computational burden. This paper also assessed the run-time performance when working with real measurements. If only 200 tracklets are tested with each other, the overall computation time stays in feasible bounds. However, the situation changes if the number of uncorrelated tracklets increases and computationally more effective methods would be required. Finally, further research must assess the quality of the obtained candidate orbits. As the here presented search is capable of finding the minimum of the loss function with predefined accuracy requirements, it is a promising approach to also get better initial orbit hypotheses.

ACKNOWLEDGMENTS

This work was funded by the Munich Aerospace scholarship program.

REFERENCES

1. DeMars K.J., Jah M.K., and Schumacher P.W. (2012). Initial Orbit Determination using Short-Arc Angle and Angle Rate Data. IEEE Transactions on Aerospace and Electronic Systems, **48**(3), 2628–2637

2. Früh C., Schildknecht T. (2009). Catalogue Correlation of Space Debris Objects. 5th European Conference on Space Debris, Darmstadt, Germany, March 30 – April 2

3. Fujimoto K., Scheeres D.J. (2010). Correlation of Optical Observations of Earth-Orbiting Objects and Initial Orbit Determination, AIAA/AAS Astrodynamics Specialist Conference, Toronto, Canada, August 2 – 5

4. Herzog J., Früh C., Schildknecht T. (2010).Build-up and maintenance of a catalogue of GEO objects with ZimSMART and ZimSMART 2, Proceedings of the International Astronautical Congress

5. Herzog J., Schildknecht T., A. Hinze, M. Ploner, A. Vananti (2013).Space Surveillance Observations at the Zimmerwald Observatory, 6th European Conference on Space Debris, Darmstadt, Germany, April 22 – 25

6. Hooke R., Jeeves T.A. (1961). Direct search solution of numerical and statistical problems, Journal of the ACM, **8**(2),212–229

7. Maruskin J.M., Scheeres D.J., Alfriend K.T. (2008). Correlation of optical observations of objects in earth orbit, Journal of Guidance,Control, and Dynamics, **32**(1),194–209

8. Milani A., Gronchi G., Vitturi M.D.M., Knezevic Z. (2004). Orbit Determination with Very Short Arcs. I Admissible Regions, Celestial Mechanics and Dynamical Astronomy, **90**,57–85

9. Press W.H., Teukolsky S.A., Vetterling W.T., Flannery B.P. (2007). Numerical Recipes: The Art of Scientific Computing, Cambridge University Press, ed. 2

10. Siminski J.A., Montenbruck O., Fiedler H., Weigel M. (2013). Best Hypotheses Search on Iso-Energy-Grid for Initial Orbit Determination and Track Association. 23rd AAS/AIAA Spaceflight Mechanics Meeting, Kauai, Hawaii, February 10 – 14

11. Tommei G., Milani A., and Rossi A. (2007). Orbit Determination of Space Debris: Admissible Regions, Celestial Mechanics and Dynamical Astronomy, **97**(4), 289 – 304